ACS NANO
Cite This: ACS Nano 2018, 12, 4494−4502
www.acsnano.org

ARTICLE

Differential Enzyme Flexibility Probed Using Solid-State Nanopores

Rui Hu,[†,‡] João V. Rodrigues,[§] Pradeep Waduge,[∥] Hirohito Yamazaki,[∥] Benjamin Cressiot,[∥] Yasmin Chishti,[⊥] Lee Makowski,[⊥] Dapeng Yu,[†,‡] Eugene Shakhnovich,[§] Qing Zhao,*[,†,‡] and Meni Wanunu*[,∥]

[†]State Key Laboratory for Mesoscopic Physics and Electron Microscopy Laboratory, School of Physics, Peking University, Beijing 100871, People's Republic of China
[‡]Collaborative Innovation Center of Quantum Matter, Beijing 100084, People's Republic of China
[§]Department of Chemistry and Chemical Biology, Harvard University, Cambridge, Massachusetts 02138, United States
[∥]Department of Physics, Northeastern University, Boston, Massachusetts 02115, United States
[⊥]Department of Bioengineering, Northeastern University, Boston, Massachusetts 02115, United States

Supporting Information

ABSTRACT: Enzymes and motor proteins are dynamic macromolecules that coexist in a number of conformations of similar energies. Protein function is usually accompanied by a change in structure and flexibility, often induced upon binding to ligands. However, while measuring protein flexibility changes between active and resting states is of therapeutic significance, it remains a challenge. Recently, our group has demonstrated that breadth of signal amplitudes in measured electrical signatures as an ensemble of individual protein molecules is driven through solid-state nanopores and correlates with protein conformational dynamics. Here, we extend our study to resolve subtle flexibility variation in dihydrofolate reductase mutants from unlabeled single molecules in solution. We first demonstrate using a canonical protein system, adenylate kinase, that both size and flexibility changes can be observed upon binding to a substrate that locks the protein in a closed conformation. Next, we investigate the influence of voltage bias and pore geometry on the measured electrical pulse statistics during protein transport. Finally, using the optimal experimental conditions, we systematically study a series of wild-type and mutant dihydrofolate reductase proteins, finding a good correlation between nanopore-measured protein conformational dynamics and equilibrium bulk fluorescence probe measurements. Our results unequivocally demonstrate that nanopore-based measurements reliably probe conformational diversity in native protein ensembles.

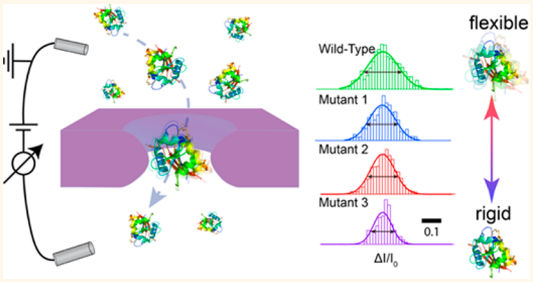

KEYWORDS: *protein flexibility, solid-state nanopore, bis-ANS, DHFR, adenylate kinase*

Proteins are known to undergo dynamic structural interconversion, rather than a static singular structure that is typically obtained from crystallography.[1] Local and collective motions of residues and subdomains in the proteins result in an ensemble of energetically similar conformational states. To complement static structural information from X-ray crystallography, alternative experimental techniques provide overwhelming evidence that protein elasticity, or flexibility, plays a fundamental role in protein activity such as enzyme catalysis,[2] signal transduction,[3] immunoglobulin interaction,[4] and intracellular protein quality control.[5,6]

Various techniques have been developed and utilized to probe protein flexibility. Fourier transform infrared spectroscopy (FTIR) and circular dichroism (CD) assess protein flexibility by probing changes in secondary structures[7] induced by a protein modification, a mutation, or a change in the protein chemical environment. The kinetics of hydrogen/deuterium (H/D) exchange upon protein exposure to deuterated solvent, probed using FTIR spectroscopy, is a useful probe of protein flexibility.[7,8] X-ray crystallography, a method capable of providing high-resolution protein structures, can access protein conformational ensemble information by providing snapshots of alternative crystal forms.[9] NMR provides atomistic detail of molecules in their crystalline and solvated states at fast time resolutions.[10] While NMR data can probe protein flexibility,[11−13] NMR spectra exhibit low resonance intensity for proteins with highly flexible structures,

Received: January 28, 2018
Accepted: April 9, 2018
Published: April 9, 2018

DOI: 10.1021/acsnano.8b00734
ACS Nano 2018, 12, 4494−4502

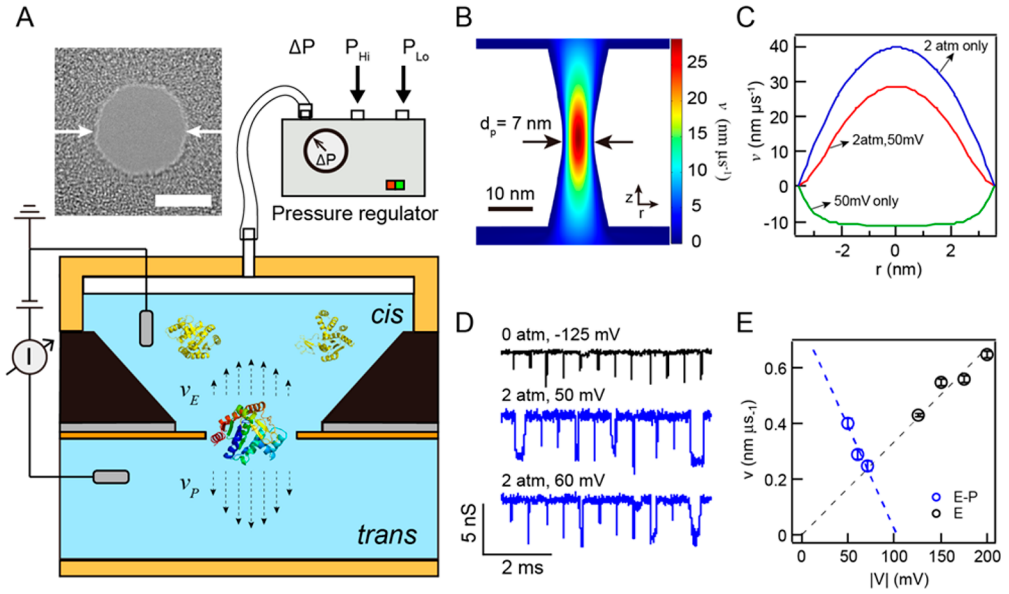

Figure 1. Pressure-driven protein transport. (A) Schematic (not-to-scale) that depicts our setup, in which feedback control between pressure-regulated air (P_{Hi}) and atmospheric air (P_{Lo}) produces an overhead air pressure atop a sealed *cis* chamber of a nanopore cell. Prior to sealing, a solution that contains a protein sample is introduced to the *cis* chamber, and an electrode is placed in contact with the solution. Set pressure (ΔP) produces volume flow across the pore toward the *trans* chamber, and an opposing electric field electrokinetically retards protein flow. The dashed arrows represent pressure-driven (v_P) and electrokinetically driven (v_E) velocities whose shape was determined from finite-element simulations. A TEM image of a 7 nm diameter silicon nitride (SiN) nanopore is shown above the schematic (scale bar = 5 nm). (B) Color contour plot of a three-dimensional finite-element COMSOL simulation of the net velocity profile around an hourglass-shaped nanopore (d_p = 7 nm, h_{eff} = 7 nm) with ΔP = 2 atm and V = +50 mV, the latter producing electro-osmotic flow from *trans* to *cis*. (C) Velocity plots along the pore profile at z = 0, the narrowest pore constriction, obtained for various conditions from the COMSOL simulation (0.4 M KCl, pH 8). Positive velocities imply flow from the *cis* chamber to the *trans* chamber. (D) Concatenated sets of analyzed AdK translocation events obtained under various indicated conditions (data digitally low-pass-filtered to 100 kHz in this presentation). (E) Extracted drift velocities (ν) as a function of absolute values of applied voltage $|V|$ for AdK transport using pressure-driven (V > 0, P > 0) and electrically driven (V < 0, P = 0) modes. Dashed lines are linear fits to the data, extrapolated to the range of the plots.

such as a molten globule state.[8] Fluorescence assays in solution can also be used as probes of protein flexibility. For example, bis-1-anilinonaphthalene-8-sulfonate (bis-ANS) has been developed as a standard fluorophore for identifying a molten globule state and for assessing protein flexibility in solution.[14−17] Weber and co-workers reported in 1969 that bis-ANS fluoresces intensely in hydrophobic environments, while less so in aqueous environments.[14,15] This results in an intense bis-ANS fluorescence in hydrophobic pockets of proteins, especially those with loose tertiary structure.[5,16,17] Single-molecule fluorescence resonance energy transfer (smFRET) has also been reported to gauge protein flexibility by analysis of the distribution of FRET values.[18,19] Potential challenges with single-molecule labeling are that (1) considerable design and control experiments are needed to dual-label a protein such that dye−dye interactions and dyes' impact on protein are minimized, and (2) orthogonal chemical approaches are required for dual labeling, which can require non-native amino acid replacements to the protein. Due to our limited understanding of the relationship between protein flexibility and protein function, it remains a formidable yet worthwhile challenge to probe intrinsic protein flexibility, preferably without having to chemically modify the protein.[8,20]

Recently, nanopore-based resistive-pulse sensing has emerged as a useful and versatile technique for label-free single-molecule detection.[21−26] In a typical setup, a pair of electrodes is used to apply a potential across the nanopore, which results in a steady-state ion current baseline. Stochastic capture and transit of macromolecules through the pore produces a set of current pulses, the characteristics of which are used to determine the analyte properties. Synthetic nanopores, due to their increased robustness and tunable geometry, have expanded the diversity of analytes to include large macromolecules in their native state. Detection of nucleic acids,[27−30] proteins,[31−48] and biomolecular complexes[49−54] have been demonstrated. Recently, our group has suggested that the breadth of fractional blockades increases with more flexible proteins by measuring a set of proteins with different α-helix (flexible) to β-sheet ratios. Full-width at half-maximum (fwhm) values obtained from Gaussian fits to the fractional blockade histograms could be an indicator of protein flexibility,[55] potentially expanding the repertoire of applications of solid-state nanopores in protein analysis.

Here, we demonstrate the ability of solid-state nanopores as a label-free, low-cost metric to probe protein flexibility based on blockade distributions. We first explore a protein system in which conformation and flexibility changes in adenylate kinase (AdK) are induced by binding a lock substrate. AdK is an abundant nucleoside monophosphate (NMP) kinase that catalyzes the reversible conversion of adenosine monophosphate (AMP) and ADP to ATP,[56] to which a bisubstrate-mimicking inhibitor, diadenosine pentaphosphate (Ap5A), binds with high affinity.[57−59] We combine pressure-driven flow and an opposing voltage bias[60,61] to retard transport and allow efficient detection of both the free and substrate-bound protein states, showing that both states can be resolved in terms of conformation and relative flexibility. Next, essential protein dihydrofolate reductase (DHFR) originated from

DOI: 10.1021/acsnano.8b00734
ACS Nano 2018, 12, 4494−4502

Escherichia coli and *Chlamydia muridarum* is probed as a prototype. DHFR plays a key role in the process of cell proliferation by reducing dihydrofolic acid to tetrahydrofolic acid, which is essential for urine and thymidylate[62] and becomes an attractive pharmaceutical cancer target.[63] We systematically study the effect of pore geometry and applied voltage on the signal for wild-type DHFR, which allows us to find the range of conditions in which pore-to-pore measurements provide consistent results. Finally, using the optimal nanopore geometry we explore the DHFR mutants with known relative flexibilities based on bulk bis-ANS fluorescence measurements,[6] finding a linear correlation between fwhm obtained from nanopore experiment and bis-ANS fluorescence intensity. Our results further highlight the promise of nanopores as label-free, simple probes of the impact of ligand binding on protein dynamics, as well as sequence-dependent protein flexibility.

RESULTS

Pressure-Assisted Transport of Adenylate Kinase. Figure 1A depicts the essential features of our experimental setup. An electron-beam fabricated nanopore was produced on a freestanding 20-nm-thick silicon nitride (SiN) membrane that is supported by a 5 × 5 mm^2 Si chip. The chip was mounted on the bottom of a sealable polyether ether ketone (PEEK) chamber using a quick-curing elastomer glue, as previously described.[64,65] The chamber was placed inside a cup that served as a *trans* chamber, and both chambers were then filled with 0.40 M KCl and 1 mM EDTA electrolyte solution buffered at pH 8 using 10 mM Tris. After injecting a sample of interest to the *cis* chamber, the chamber was sealed and connected to a computer-controlled pressure regulator, which uses feedback electronics to maintain a pressure gradient ΔP by balancing two valve inputs, one being house-compressed air at ∼6 bar air pressure (P_{Hi}) and the other being atmospheric air (P_{Lo}). Two Ag/AgCl electrodes inserted into the *cis* and *trans* chambers were connected to a high-bandwidth Chimera Instruments VC100 current amplifier system,[44,55] and voltage bias was applied to the *trans* chamber, keeping the *cis* chamber as the ground electrode. The scheme shows the most elaborate case in which pressure and voltage are simultaneously applied in order to provide opposing driving gradients: pressure-driven flow is used to drive protein transport, and voltage-induced electrophoresis (and/or electro-osmosis) is used to retard transport and gain signal. A simpler mode of transport in which only voltage is used to drive protein transport, equaling $\Delta P = 0$, in which case ν_E is the dominant driving mode, is not shown here for brevity.

Based on its amino acid contents, AdK is a negatively charged protein (p$I \approx 5.76$, $q_{AdK} \approx -4.9e$ at pH 8.0). However, using voltage-driven transport, translocation signals are only observed at negative bias values, which suggests that the dominant driving force for transport is electro-osmotic, rather than electrophoretic.[55,66] Hence, in our pressure-driven transport experiments, an applied positive voltage is used to electrokinetically retard transport, against the pressure-driven volume flow. Simulation of the velocity profile inside the nanopore under pressure flow and retarding the electric field provides insight into the magnitude of velocities that is obtained, as shown in Figure 1B (see also SI-1). The contour plot shows the two-dimensional velocity (ν) profile inside and near a 7 nm diameter nanopore at $\Delta P = 2.0$ atm and $V = +50$ mV. A positive value of ν indicates flow from the *cis* (top) chamber to the *trans* (bottom) chamber. Figure 1C displays the calculated ν profile along the horizontal axis at the narrowest nanopore constriction ($z = 0$) using $V = 50$ mV (electric field only, green), $\Delta P = 2.0$ atm (pressure only, blue), and $\Delta P = 2.0$ atm with $V = +50$ mV (pressure-assisted, red). From these results we see that pressure-driven flow at 2.0 atm (ν_P) results in ∼4-fold greater velocities than electro-osmotic velocity at 50 mV voltage (ν_E).

Figure 1D compares concatenated sets of ion current traces obtained from electrically facilitated (black) and pressure-driven (blue) transport of AdK, respectively. While electrically facilitated translocations appear as short and sharp pulses with durations of 10−20 μs, pressure-assisted translocations are longer (∼100 μs) and the events have higher amplitudes and appear more pronounced. Figure 1E shows the drift velocities, ν, extracted from fitting the dwell-time histograms to a 1D drift-diffusion model[44] for different AdK transport experiments conducted on the same pore. Values of ν obtained from pressure-driven translocations ($\nu_{P\text{-}E}$) are marked in blue and correspond to voltages shown on the bottom axis, while values obtained from electrically facilitated translocations (ν_E) are marked in black, corresponding to voltages shown on the top axis. As expected, velocities for pressure-driven transport decrease for increasing retarding voltages, while electrically facilitated transport results in increasing velocities with voltage. While pressure-driven transport with opposing voltage can be used to retard transport kinetics and improve the signal quality, we found that translocations were rare for $V_{E\text{-}P} > 70$ mV, possibly because of an insufficient driving force exerted on the molecules. Similarly, electrically facilitated translocations were not observed at voltages below $|V_E| < 125$ mV, possibly due to inefficient capture resulting from entropy-overcome failure.[39,67]

Discrimination of AdK-apo and AdK-Ap5A: Transport Dynamics, Conformation, and Flexibility. After having optimized the conditions for observing AdK transport, we investigated the structural impact of AdK binding to a lock substrate. AdK-apo, the substrate-free form of the enzyme, consists of three domains, as shown in Figure 2A (left): (1) the core domain comprising the central β-sheet with six surrounding α-helices, shown in blue; (2) the AMP-binding domain termed NMP, shown in green; and (3) a lid-like ATP-binding domain termed LID, shown in gray. Ap5A, as a bisubstrate-mimicking inhibitor of AdK, simultaneously occupies both binding sites of ATP and ADP,[57] locking the enzyme tightly in a closed conformation ($k_d \approx 450$ nM).[68] Figure 2A also describes the conformational change of AdK-apo upon binding Ap5A, where the "open form" closes to a "closed form", and the LID and NMP domains move inward to form a pocket that holds Ap5A inside.[58]

Changes in transport dynamics upon AdK-apo binding to Ap5A are revealed by changes in the values of drift velocities (ν), capture rates (R), and diffusion coefficients (D), as shown in Figure 2B−D, respectively (scatter plots for all experiments are shown in Figure S2). First, we find that $\nu_{P\text{-apo}}$ decreases with retarding electric field (linear trendline shown as a dashed line), while $\nu_{P\text{-Ap5A}}$ increases with retarding electric field. A similar trend was observed for the capture rates R (Figure 2C), in which decreases in R were observed with retarding voltage for AdK-apo and increases in R were observed for AdK-Ap5A. These observations both point to the added charge of AdK upon binding Ap5A: a more negative charge ($q_{Ap5A} \approx -5e$) shifts the electrokinetic balance from a dominantly electro-osmotic retarding mechanism to an electrophoretic enhancing

DOI: 10.1021/acsnano.8b00734
ACS Nano 2018, 12, 4494−4502

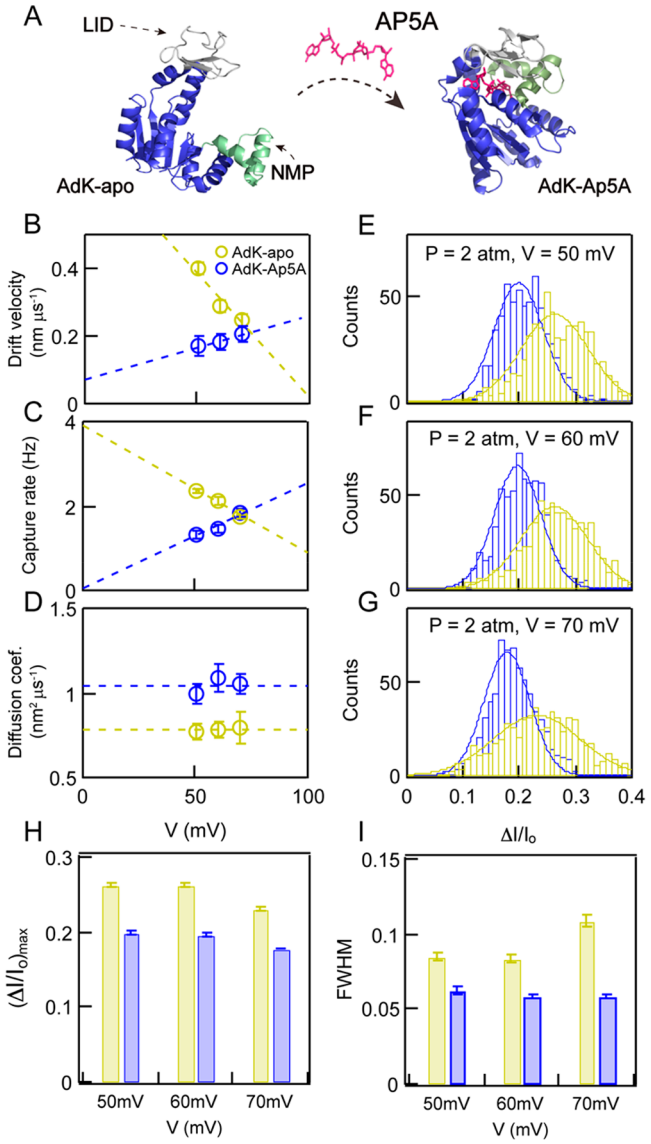

Figure 2. Adenylate kinase (AdK) size and flexibility changes upon binding to a lock substrate, Ap5A. (A) PDB-based cartoons depicting the three subdomains of AdK, as well as its conformational change upon binding a lock substrate (structure of AdK-apo from PDB ID 4AKE, structure of AdK-Ap5A from PDB ID 1AKE). (B–D) Drift velocities (ν), capture rates (R), and diffusion coefficients (D) as a function of retarding voltage (V) during pressure-driven transport of AdK-apo (yellow markers) and Ap5A (blue markers). (E–G) Fractional current blockade ($\Delta I/I_0$) distributions of AdK-apo (yellow bars) and AdK-Ap5A (blue bars) at ΔP = 2 atm for V = 50, 60, and 70 mV, respectively. (H, I) Mean fractional current blockades $\langle \Delta I/I_0 \rangle$ and fwhm's extracted from Gaussian fits to $\Delta I/I_0$ distributions for the experiments above, respectively.

mechanism, such that a retarding voltage in AdK-apo is actually an enhancing voltage in AdK-Ap5A, which leads to higher capture rates and velocities with increasing voltages. Additionally, values of D, shown in Figure 2D, are voltage independent for both AdK-apo and AdK-Ap5A, for which the values were 0.79 ± 0.01 nm^2/μs and 1.04 ± 0.04 nm^2/μs, respectively. The lower D for AdK-Ap5A is consistent with a more compact protein structure. To gauge the relative size and conformational flexibility of AdK, we analyzed the electrical pulse amplitude statistics. Histograms of $\Delta I/I_0$ and corresponding Gaussian fits for AdK-apo and AdK-Ap5A for pressure-driven transport with retarding voltages of 50, 60, and 70 mV are shown in Figure 2E–G, respectively. Consistently, the mean $\langle \Delta I/I_0 \rangle$ values of AdK-Ap5A are lower than those of AdK-apo, indicating a reduction in the protein's globular size upon binding to Ap5A.[58] In addition, the distributions of AdK-Ap5A are visually narrower than that of AdK-apo, indicating that the substrate-locked state is conformationally less flexible. We found that the $\Delta I/I_0$ data fit well to Gaussian distributions for all experiments, and based on these fits we extracted the values of $\langle \Delta I/I_0 \rangle$ and fwhm, shown in Figure 2H and I, respectively. Throughout the voltage range tested, we find a consistent value of $\langle \Delta I/I_0 \rangle$ = 0.25 ± 0.01 for AdK-apo and 0.19 ± 0.01 for AdK-Ap5A, respectively. Based on these values, hydrodynamic radii R_H of 2.88 ± 0.2 nm for AdK-apo and 2.19 ± 0.2 nm for AdK-Ap5A were calculated,[44,55,69] highlighting the huge impact of the lock substrate on the protein conformation.[58] Further, the fwhm values summarized in Figure 2I for AdK-apo (0.093 ± 0.012) and AdK-Ap5A (0.059 ± 0.002) point to the more conformationally flexible structure of the free protein, as compared with its lock-substrate complex. It should be noted that the fwhm value of AdK-apo at 70 mV is relatively higher, and $\langle \Delta I/I_0 \rangle$ is slightly smaller, as compared to these values at 50 and 60 mV and that the source of this deviation is not currently understood.

Influence of Voltage and Pore Geometry on Protein Pulse Statistics. Prior to our comparative study of a set of DHFR mutants, we explored the influence of applied voltage and pore geometry on the signal for the same protein, in this case the dihydrofolate reductase mutant L28R originated from *E. coli*. In the case of DHFR, a pressure/voltage combination was not necessary to slow down transport, so instead we used the traditional voltage-driven mode. In Figure 3A, we show two-dimensional $\Delta I/I_0$ *vs* dwell time contour plots for the DHFR mutant L28R driven through a d_p = 4.3 nm, h_{eff} = 7 nm pore at different voltages in the range −125 to −300 mV (0.35 M NaCl, 10 mM Tris, 1 mM EDTA, 10 mM DTT, pH 8). Similar to AdK, electro-osmosis rather than electrophoresis is predominate in this case ($q_{DHFR} \approx -9.7e$ at pH 8, p$I \approx 5.99$). Corresponding $\Delta I/I_0$ histograms are shown to the right of each contour plot. While for the most part the $\Delta I/I_0$ distributions appear similar, significant broadening is observed for voltages above 225 mV, most likely due to an artifact arising from bandwidth limitations[51] (arrows in Figure 3A show artifactual $\Delta I/I_0$ broadening for events below 4 μs). Figure 3B displays a concatenated representative set of translocation events detected at −125, −175, and −300 mV, in which the event durations clearly decrease as voltage is increased. We fit the event duration histogram using $\sim\exp(-x/\tau)$ and found that characteristic duration time τ is inversely proportional to the applied voltage (see Figure S3). Figure 3C shows that the diameter of the nanopore (d_p) remains constant during the experiment, as calculated from the open pore current using a previously described equation.[44] Figure 3D shows the values of $\langle \Delta I/I_0 \rangle$ as a function of $|V|$, which also remain independent of voltage ($\langle \Delta I/I_0 \rangle$ = 0.35 ± 0.02). Figure 3E shows that the fwhm values slightly increase (~20%) as a function of $|V|$, clearly an artifact caused by the limited time resolution of our measurements at high voltages, which results in clear broadening of $\Delta I/I_0$ values. Another data set carried out for a more flexible wide-type (wt) DHFR originated from *C. muridarum* (see Figure S4) shows that fwhm values are voltage

DOI: 10.1021/acsnano.8b00734
ACS Nano 2018, 12, 4494–4502

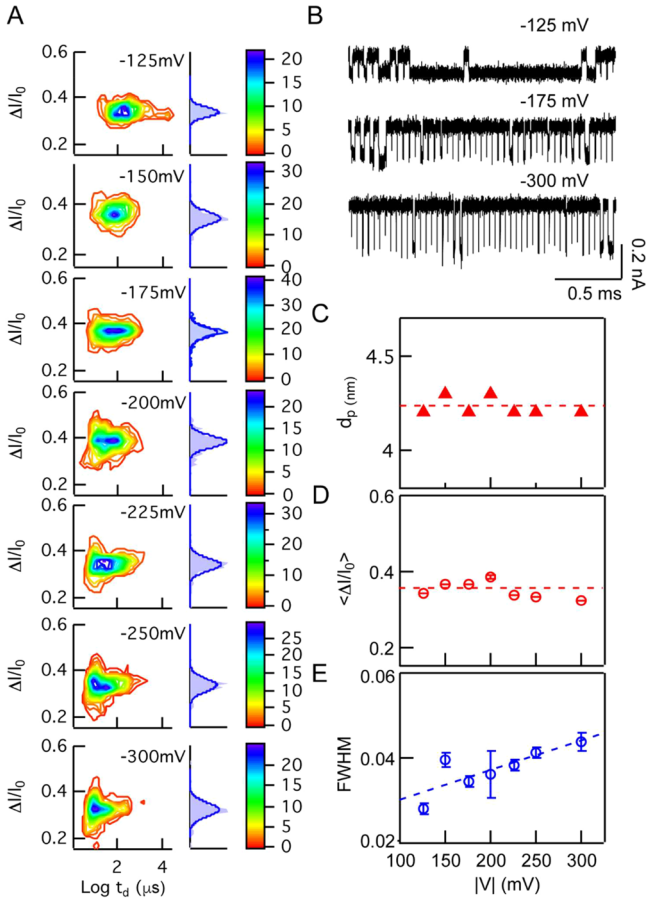

Figure 3. Voltage dependence on protein signal characteristics. (A) Color contour plots of $\Delta I/I_0$ *vs* log dwell times (t_d) for dihydrofolate reductase (DHFR) mutant L28R at indicated voltages. To the right of each contour plot is a normalized $\Delta I/I_0$ histogram (light blue bars) fit to a Gaussian distribution (dark blue curve). (B) Representative concatenated sets of DHFR-E1 translocations detected at −125, −175, and −300 mV (data low-pass filtered to 250 kHz). (C−E) Pore diameters, mean fractional current blockades, and fwhm values as a function of applied voltage, respectively.

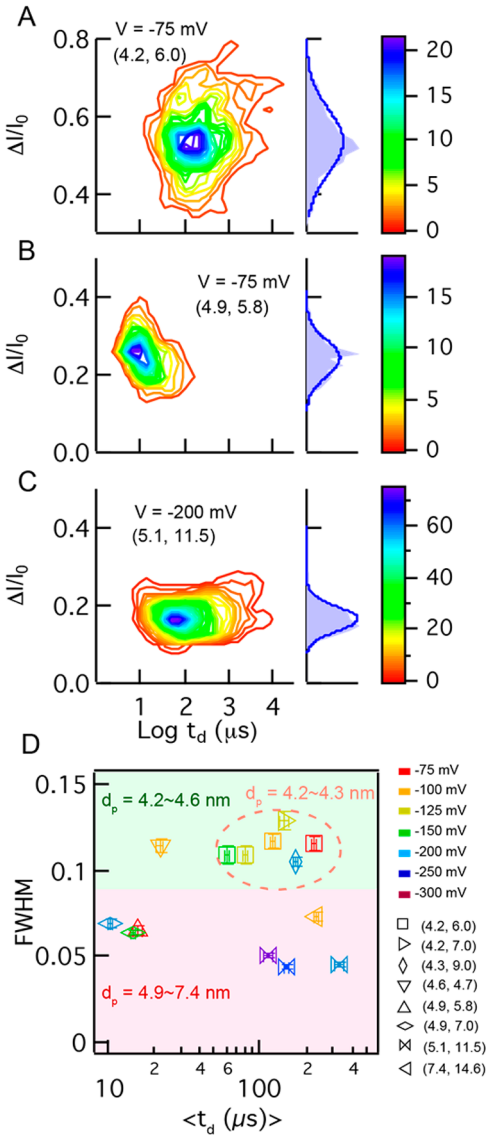

Figure 4. Influence of pore geometry on DHFR signal characteristics. (A−C) Color contour plots of $\Delta I/I_0$ *vs* log(t_d) for DHFR mutant C7, as well as normalized $\Delta I/I_0$ distributions shown to the right of each plot, obtained from nanopores with different geometries indexed as (d_p, h_{eff}) in each plot. The *y*-axis scales are set to the same height (though not the same values). (D) Summary plot of fwhm and mean t_d values obtained from eight different nanopores at various voltages (coded by colors in the legend). Data are bisected to two regions on the plot based on pore diameter, which shows that 4.2−4.6 nm pores (green-shaded area) provide consistent fwhm values, and in the range 4.2−4.3 nm, consistent dwell times are obtained as well (dashed orange circle).

independent in the range |*V*| = 200 to 300 mV. Overall, these findings suggest for DHFR that lower voltages result in more stable and reliable measurements, less prone to artifacts of time resolution.

While we have found the measured pulse parameter statistics to be stable as a function of voltage for a particular protein, significant deviations were observed as a function of the pore geometry. In Figure 4A−C we show 2D contour plots and corresponding $\Delta I/I_0$ histograms, in which the data for wt DHFR were acquired in three independent pores with dimensions indicated as (d_p, h_{eff}). The *y*-axis scales in Figure 4A−C were set to the same height (though not the same values), in order to illustrate the impact of pore dimensions on the distribution breadth. Clearly, dwell times also vary significantly as a function of the pore geometry: For the (4.9, 5.8) pore in Figure 4B, events faster than ∼5 μs appear to be distorting the contour plot, while in a thicker pore (5.1, 11.5), shown in Figure 4C, the dwell times vary over 3 orders of magnitude. A more detailed view of the effect of pore geometry is shown in Figure 4D, where we detected wt DHFR using eight pores of different geometry at different voltages (see legend for voltage and pore identifiers). We find two distinct populations, the first consisting of data points with average fwhm's of 0.114 ± 0.008 and the second containing data points with fwhm values of 0.058 ± 0.011. What clearly bisects these populations is the pore diameter, which was in the range of 4.2−4.6 nm for population 1, while being 4.9 to 7.4 nm in population 2. For similar pore diameters and voltages, we find that dwell times increase for thicker pores and that a finely tuned pore diameter produces reproducible results, as shown in the dashed circle for three pores in the range 4.2 < d_p < 4.3 nm.

DOI: 10.1021/acsnano.8b00734
ACS Nano 2018, 12, 4494−4502

Identifying this consistency range was critical for our measurements of multiple proteins.

Conformational Flexibility of DHFR Mutants. After identifying the experimental conditions under which we obtain consistent nanopore results, we systematically studied the flexibilities of different DHFR mutants and compared the results to bis-ANS fluorescence intensity measurements, a good metric for protein conformational flexibility (representative current traces are shown in Figure S5). Specifically, we used relative bis-ANS fluorescence intensity values recently published for drug-resistant DHFR variants.[6] Figure 5A shows the binding pocket of DHFR in the view of the zoom-in cartoon (PDB ID 5DFR). A total of nine DHFR mutants originating from *E. coli* and *C. muridarum* were used here (the sequences for wt DHFR originating from these two organisms are shown in Materials and Methods), in which the mutated residues are chosen within a short region in the binding pocket, colored in red. Figure 5B shows the bis-ANS normalized intensity of each mutant in an ascending order.[6] The mutants L28R, P21L, P21L/A26T, and A26T originated from *E. coli* (labeled as E1, E2, E3, and E4, respectively), while the mutants L30R, E28T/L30R, WT, P23L/E28T/L30R, and E28T originated from *C. muridarum* (labeled as C5, C6, C7, C8, and C9, respectively). These nine mutants were carefully selected from a larger set of tested DHFR mutants, in order to cover a wide range of bis-ANS values. Figure 5C displays the typical $\Delta I/I_0$ histograms of mutants C7, C6, C5, and E4, obtained from pore 1 (4.3, 9.0). Narrower distributions were obtained for samples with smaller bis-ANS values; for example, E4 has a tighter $\Delta I/I_0$ distribution than C7. For comparison, the distribution of 1 kbp dsDNA for a pore with the same dimensions is much tighter than for any of the proteins (fwhm = 0.024 ± 0.01), indicating the relatively more robust double-helical structure of DNA than proteins.[70]

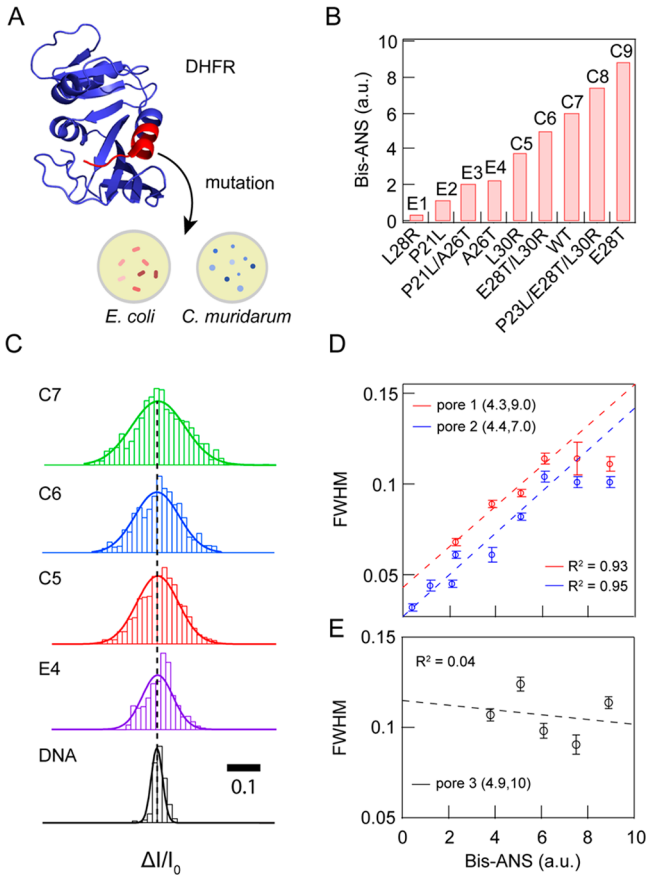

Figure 5. Correlation of DHFR mutant conformational flexibilities with bulk fluorescence data. (A) PDB-based cartoon of DHFR (PDB ID 5DFR). The region for which we probed various mutants is shown in red. (B) Bis-ANS fluorescence intensities (relative to wt *E. coli* DHFR) for a set of nine DHFR mutants originating from *E. coli* and *C. muridarum*, arranged in ascending order of bis-ANS fluorescence, a reporter of protein flexibility. (C) Comparative display of $\Delta I/I_0$ distributions and corresponding Gaussian fits for mutants C7, C6, C5, and E4 (acquired at −100 mV from pore 1, data filtered to 250 kHz), as well as 1 kbp double-stranded DNA for comparison (acquired at 300 mV from a nanopore with the same dimensions, filtered to 250 kHz). (D) Correlation between fwhm values and bis-ANS data for two independent pores with indicated geometric parameters, pore 1 (R^2 = 0.93) and pore 2 (R^2 = 0.95). All data were low-pass filtered to 200 kHz. (E) Correlation between fwhm values and bis-ANS data for pore 3 (R^2 = 0.04), showing the inadequate resolution of a larger pore.

In Figure 5D, we show a highly linear correlation between fwhm values and normalized bis-ANS values by two independent experiments from pore 1 (4.2, 9.0) and pore 2 (4.4, 7.0) with linear coefficient R^2 = 0.93 for pore 1 and R^2 = 0.95 for pore 2. It should be noted that a plateau appears at large bis-ANS values, likely due to a limited range of flexibilities that can be observed using nanopores in this diameter range, as previously observed.[55] Therefore, we omitted the last two points for the linear fit. For comparison, in Figure 5E we present data for a third pore with a diameter of 4.9 nm, as well as a linear fit to the data (R^2 = 0.04), which shows no correlation between fwhm values and bis-ANS data due to inadequate measurement time resolution. We note that while using thinner pores provides a superior resolution, nanopores fabricated in thin silicon nitride (SiN) do expand progressively during the experiment.[65] To avoid this influencing our measurements, we repeated the protein measurements for the data sets in different orders, which confirms that the data are a reflection of protein behavior, rather than pore artifacts.

CONCLUSION

Proteins are life's most sophisticated molecules because they are capable of doing chemical and mechanical work in a highly specific manner. In this work, we systematically demonstrate that nanopores can be used to gain information about a conformational ensemble of proteins that can be critical for their function. Using a combination of nanopores of finely tuned geometrical features,[55] pressure−voltage competition to slow down proteins,[60,61] and high-bandwidth low-noise ion current detection,[44] we overcome the challenge of detecting ultrafast protein transport[43] to provide meaningful information about unlabeled/untethered proteins in their native state. We have shown here that AdK binding to a lock substrate, Ap5A, results in a tighter and less dynamically flexible shape, as evidenced by the current amplitude spike statistics collected from passing ∼1000 molecules. Extensive conformational dynamics in the free Adk protein were observed, indicated by a large fwhm of the ion current signal distributions, while the Ap5A-bound protein was found to be smaller and less flexible, as consistent with small-angle X-ray scattering experiments.[59]

In order to study subtler changes in various DHFR mutants, we performed an extensive study of the influence of applied voltage and pore geometry on the protein signals. We found that applied voltage minimally influences fwhm values, unless

DOI: 10.1021/acsnano.8b00734
ACS Nano 2018, 12, 4494−4502

the signals are convolved with the limited time resolutions at high driving forces (in this case a high voltage), in which case overestimated values of fwhm are obtained.[51] Similarly, using pores that are too large, for example, degrades the signal sensitivity to protein flexibility *via* fast transport times that are difficult to detect reliably. Finally, we demonstrated using optimum-shape nanopores a linear correlation between bis-ANS fluorescence values from bulk measurements and nanopore-based fwhm values. These results confirm that conformational flexibility in proteins of similar primary structure, which can vary substantially, can be efficiently detected at nanomolar-level concentrations without any chemical labels or chemistry applied to the protein, allowing a rapid assessment of the impact of mutations in a protein on its conformational diversity. Our label-free, fast, and straightforward approach that uses a solid-state nanopore-based sensor could find uses in drug-screening applications,[71] as well as in deciphering paradigms in structure−flexibility−function correlations, for example, activation pathways in allosteric proteins.[72]

MATERIALS AND METHODS

Nanopore Fabrication and Measurement. The chips we used here were 5 × 5 mm^2 Si substrates preoxidized to form a 2.5 μm thick thermal SiO_2 dielectric barrier layer, onto which a 50-nm-thick LPCVD low-stress SiN_x film was deposited on both sides. After photolithography and developing, a Technics Micro-RIE series 800 etcher was used to remove 50 nm of SiN_x in a photolithographically patterned region using sulfur hexafluoride (SF_6) (300 mTorr, 150 W), and the 2.5 μm SiO_2 was etched by a subsequent buffered oxide etch consisting of one part 49% HF and six parts 40% NH_4F (1:6 BOE). Then a freestanding 50 nm SiN_x membrane was formed after anisotropic KOH (40% w/w, 70 °C) etching and exposing in 1:6 BOE again to remove the other layer of 2.5 μm of SiO_2 on the membrane. The effective thickness of the freestanding SiN_x membrane was controlled by timed RIE with an etching rate of 9.0 Å/s prior to drilling and calibrated by 1 kbp DNA translocation before the protein detection experiment.

Nanopores fabricated using a transmission electron microscope (JEOL 2010FEG, 200 kV) on a SiN_x membrane were cleaned using a hot piranha solution (1:3 H_2O_2/H_2SO_4), followed by several rinse cycles using hot deionized water. After drying using nitrogen flow, the chips were mounted in a homemade sealable *cis* chamber using a quick-curing elastomer gasket (Smooth-on Ecoflex 00-35) to reduce the capacitance to below 100 pF.[64] For pressure-assisted experiments, the *cis* chamber was sealed by connecting an air pressure inlet that is pressure-regulated using a LabVIEW-based pressure-control system. For electrically facilitated experiments (P = 0), the *cis* chamber was kept open to the atmosphere.

AdK Production/Purification. Plasmid for human recombinant AdK (pEAK91) was obtained from Magnus Wolf-Watz (Umea, Sweden), followed by a standard purification method. Ap5A was obtained from Sigma-Aldrich.

AdK Conformational Change Experiment. The experiments with AdK were carried out using 0.4 M KCl, 10 mM Tris, and 1 mM EDTA electrolyte solution at pH 8. The homemade Ag/AgCl electrodes equipped with each chamber were connected to a Chimera Instruments VC100 amplifier system with a sampling rate of 4.17 MHz for data collection.[44] Calibration of the pore geometry was performed by measuring blockade amplitudes using 1 kbp double-stranded DNA. Then, proteins were added and mixed into desired concentration (125 nM) using a pipet in the *cis* chamber. A substantial number of protein translocation events (n > 600) were collected, while continuously monitoring the open current value to ensure that no significant pore size changes occurred during the measurement. Ap5A was added to a ratio of Ap5A:AdK = 10:1 before measuring the complex properties. Data were collected using Chimera Instruments VC100 at a sampling rate of 4.17 MHz, analyzed using Pythion (https://github.com/rhenley/Pyth-Ion) after applying a digital low-pass filter of 150 kHz.

Purification of DHFR. DHFR variants + C-terminal His-tag were overexpressed in *E. coli* BL21 cells transformed with pFLAG plasmids and purified using chelating Ni-NTA columns followed by size exclusion chromatography separation as described in ref 6. Reported bis-ANS fluorescence intensity values are relative to wild-type *E. coli* DHFR. The sequence of wt DHFR originated from *E. coli* is MISLIAALAVDRVIGMENAMPWNLPADLAWFKRNTLNKPVIMGRHTWESIGRPLPGRKNIILSSQPGTDDRVTWVKSVDEAIAACGDVPEIMVIGGGRVYEQFLPKAQKLYLTHIDAEVEGDTHFPDYEPDDWESVFSEFHDADAQNSHSYCFEILERRHHHHHH, while the sequence of wt DHFR originated from *C. muridarum* (C7) is MIQATGIVAIDPRGVMGGAGKLPWNYPEDLRFFSETIQDHPIIMGRKTWESLPDRYKCGRTVIVFSRQHSCAQGIWISSLVEYEKLSLNSPFLIGGAELFDWFFQYNLLKSCFVTHIKREYQGDTFFPVERLSGWKRESVLKTEDFNIYHYENYANQNPGSHHHHHH.

Bis-ANS Fluorescence Assays for DHFR Mutants. Reported bis-ANS fluorescence intensity values are relative to wild-type *E. coli* DHFR.[6] We monitored the bis-ANS fluorescence intensity change during proteolytic degradation with a set of *E. coli* DHFR mutants (see Figure S6) and performed fluorescence-based bis-ANS titrations of three DNFR variants (see Figure S7), showing that bis-ANS fluorescence intensity data reflect the proportion of highly flexible intermediates in solution.

Detection of DHFR Mutants. DHFR mutants were detected in 0.35 M NaCl, 10 mM Tris, 1 mM EDTA, and 10 mM DTT electrolyte solution at pH 8 (DDT was used to inhibit protein aggregation). Data were collected using a Chimera Instruments VC100 at a sampling rate of 4.17 MHz, analyzed using Pythion after applying a digital low-pass filter of 250 kHz.

ASSOCIATED CONTENT

Supporting Information

The Supporting Information is available free of charge on the ACS Publications website at DOI: 10.1021/acsnano.8b00734.

Additional information (PDF)

AUTHOR INFORMATION

Corresponding Authors

*E-mail: zhaoqing@pku.edu.cn.
*E-mail: wanunu@neu.edu.

ORCID

João V. Rodrigues: 0000-0002-5605-656X
Benjamin Cressiot: 0000-0001-9319-3152
Lee Makowski: 0000-0003-0202-9264
Qing Zhao: 0000-0003-3374-6901
Meni Wanunu: 0000-0002-9837-0004

Notes

The authors declare no competing financial interest.

ACKNOWLEDGMENTS

This work was supported by National Science Foundation NSF/MCB-1645671 (R.H., P.W., H.Y., B.C., M.W.), NSF/MCB-1158340 (Y.C., L.M.), and National Natural Science Foundation of China NSFC 51622201, 61571015, and 91733301 (R.H., D.Y., Q.Z.).

REFERENCES

(1) Jorgensen, W. L. Rusting of the Lock and Key Model for Protein-Ligand Binding. *Science* **1991**, *254*, 954−955.

DOI: 10.1021/acsnano.8b00734
ACS Nano 2018, 12, 4494−4502

(2) Kokkinidis, M.; Glykos, N. M.; Fadouloglou, V. E. Protein Flexibility and Enzymatic Catalysis. *Adv. Protein Chem. Struct. Biol.* **2012**, *87*, 181−218.
(3) Brueschweiler, S.; Schanda, P.; Kloiber, K.; Brutscher, B.; Kontaxis, G.; Konrat, R.; Tollinger, M. Direct Observation of the Dynamic Process Underlying Allosteric Signal Transmission. *J. Am. Chem. Soc.* **2009**, *131*, 3063−3068.
(4) Sondermann, P.; Pincetic, A.; Maamary, J.; Lammens, K.; Ravetch, J. V. General Mechanism for Modulating Immunoglobulin Effector Function. *Proc. Natl. Acad. Sci. U. S. A.* **2013**, *110*, 9868−72.
(5) Bershtein, S.; Mu, W.; Serohijos, A. W. R.; Zhou, J.; Shakhnovich, E. I. Protein Quality Control Acts on Folding Intermediates to Shape the Effects of Mutations on Organismal Fitness. Mol. *Mol. Cell* **2013**, *49*, 133−144.
(6) Rodrigues, J. V.; Bershtein, S.; Li, A.; Lozovsky, E. R.; Hartl, D. L.; Shakhnovich, E. I. Biophysical Principles Predict Fitness Landscapes of Drug Resistance. *Proc. Natl. Acad. Sci. U. S. A.* **2016**, *113*, E1470−8.
(7) Celej, M. S.; Montich, G. G.; Fidelio, G. D. Protein Stability Induced by Ligand Binding Correlates with Changes in Protein Flexibility. *Protein Sci.* **2003**, *12*, 1496−1506.
(8) Park, S. J.; Borin, B. N.; Martinez-Yamout, M. A.; Dyson, H. J. The Client Protein P53 Adopts a Molten Globule-Like State in the Presence of Hsp90. *Nat. Struct. Mol. Biol.* **2011**, *18*, 537−41.
(9) Fraser, J. S.; van den Bedem, H.; Samelson, A. J.; Lang, P. T.; Holton, J. M.; Echols, N.; Alber, T. Accessing Protein Conformational Ensembles Using Room-Temperature X-Ray Crystallography. *Proc. Natl. Acad. Sci. U. S. A.* **2011**, *108*, 16247−52.
(10) Roberts, G. C.; Jardetzky, O. Nuclear Magnetic Resonance Spectroscopy of Amino Acids, Peptides, and Proteins. *Adv. Protein Chem.* **1970**, *24*, 447−545.
(11) Salmon, L.; Bouvignies, G.; Markwick, P.; Blackledge, M. Nuclear Magnetic Resonance Provides a Quantitative Description of Protein Conformational Flexibility on Physiologically Important Time Scales. *Biochemistry* **2011**, *50*, 2735−2747.
(12) Helmus, J. J.; Surewicz, K.; Surewicz, W. K.; Jaroniec, C. P. Conformational Flexibility of Y145stop Human Prion Protein Amyloid Fibrils Probed by Solid-State Nuclear Magnetic Resonance Spectroscopy. *J. Am. Chem. Soc.* **2010**, *132*, 2393−2403.
(13) Woody, R. W.; Clark, D. C.; Roberts, G. C. K.; Martin, S. R.; Bayley, P. M. Molecular Flexibility in Microtubule Proteins-Proton Nuclear Magnetic-Resonance Chracterization. *Biochemistry* **1983**, *22*, 2186−2192.
(14) Takashi, R.; Tonomura, Y.; Morales, M. F. 4,4'-Bis (1-Anilinonaphthalene 8-Sulfonate) (Bis-Ans): A New Probe of the Active Site of Myosin. *Proc. Natl. Acad. Sci. U. S. A.* **1977**, *74*, 2334−8.
(15) Rosen, C. G.; Weber, G. Dimer Formation from 1-Anilino-8-Naphthalenesulfonate Catalyzed by Bovine Serum Albumin: A New Fluorescent Molecule with Exceptional Bindind Properties. *Biochemistry* **1969**, *8*, 3915.
(16) Goldberg, M. E.; Semisotnov, G. V.; Friguet, B.; Kuwajima, K.; Ptitsyn, O. B.; Sugai, S. An Early Immunoreactive Folding Intermediate of the Tryptophan Synthease Beta 2 Subunit Is a ' Molten Globule'. *FEBS Lett.* **1990**, *263*, 51−56.
(17) Jones, B. E.; Jennings, P. A.; Pierre, R. A.; Matthews, C. R. Development of Nonpolar Surfaces in the Folding of *Escherichia Coli* Dihydrofolate Reductase Detected by 1-Anilinonaphthalene-8-Sulfonate Binding. *Biochemistry* **1994**, *33*, 15250−15258.
(18) Majumdar, D. S.; Smirnova, I.; Kasho, V.; Nir, E.; Kong, X.; Weiss, S.; Kaback, H. R. Single-Molecule FRET Reveals Sugar-Induced Conformational Dynamics in Lacy. *Proc. Natl. Acad. Sci. U. S. A.* **2007**, *104*, 12640−12645.
(19) Murphy, M. C.; Rasnik, I.; Cheng, W.; Lohman, T. M.; Ha, T. J. Probing Single-Stranded DNA Conformational Flexibility Using Fluorescence Spectroscopy. *Biophys. J.* **2004**, *86*, 2530−2537.
(20) Tzeng, S.-R.; Kalodimos, C. G. Dynamic Activation of an Allosteric Regulatory Protein. *Nature* **2009**, *462*, 368−372.
(21) Kasianowicz, J. J.; Brandin, E.; Branton, D.; Deamer, D. W. Characterization of Individual Polynucleotide Molecules Using a Membrane Channel. *Proc. Natl. Acad. Sci. U. S. A.* **1996**, *93*, 13770−13773.
(22) Sutherland, T. C.; Long, Y. T.; Stefureac, R. I.; Bediako-Amoa, I.; Kraatz, H. B.; Lee, J. S. Structure of Peptides Investigated by Nanopore Analysis. *Nano Lett.* **2004**, *4*, 1273−1277.
(23) Oukhaled, G.; Mathe, J.; Biance, A. L.; Bacri, L.; Betton, J. M.; Lairez, D.; Pelta, J.; Auvray, L. Unfolding of Proteins and Long Transient Conformations Detected by Single Nanopore Recording. *Phys. Rev. Lett.* **2007**, *98*, 4.
(24) Soskine, M.; Biesemans, A.; Maglia, G. Single-Molecule Analyte Recognition with ClyA Nanopores Equipped with Internal Protein Adaptors. *J. Am. Chem. Soc.* **2015**, *137*, 5793−5797.
(25) Van Meervelt, V.; Soskine, M.; Singh, S.; Schuurman-Wolters, G. K.; Wijma, H. J.; Poolman, B.; Maglia, G. Real-Time Conformational Changes and Controlled Orientation of Native Proteins inside a Protein Nanoreactor. *J. Am. Chem. Soc.* **2017**, *139*, 18640−18646.
(26) Piguet, F.; Ouldali, H.; Pastoriza-Gallego, M.; Manivet, P.; Pelta, J.; Oukhaled, A. Identification of Single Amino Acid Differences in Uniformly Charged Homopolymeric Peptides with Aerolysin Nanopore. *Nat. Commun.* **2018**, *9*, in press DOI: 10.1038/s41467-018-03418-2.
(27) Li, J.; Gershow, M.; Stein, D.; Brandin, E.; Golovchenko, J. A. DNA Molecules and Configurations in a Solid-State Nanopore Microscope. *Nat. Mater.* **2003**, *2*, 611−5.
(28) Henley, R. Y.; Ashcroft, B. A.; Farrell, I.; Cooperman, B. S.; Lindsay, S. M.; Wanunu, M. Electrophoretic Deformation of Individual Transfer RNA Molecules Reveals Their Identity. *Nano Lett.* **2016**, *16*, 138−144.
(29) Shekar, S.; Niedzwiecki, D. J.; Chien, C. C.; Ong, P.; Fleischer, D. A.; Lin, J. X.; Rosenstein, J. K.; Drndic, M.; Shepard, K. L. Measurement of DNA Translocation Dynamics in a Solid-State Nanopore at 100 ns Temporal Resolution. *Nano Lett.* **2016**, *16*, 4483−4489.
(30) Alibakhshi, M. A.; Halman, J. R.; Wilson, J.; Aksimentiev, A.; Afonin, K. A.; Wanunu, M. Picomolar Fingerprinting of Nucleic Acid Nanoparticles Using Solid-State Nanopores. *ACS Nano* **2017**, *11*, 9701−9710.
(31) Fologea, D.; Ledden, B.; McNabb, D. S.; Li, J. Electrical Characterization of Protein Molecules by a Solid-State Nanopore. *Appl. Phys. Lett.* **2007**, *91*, 539011−539013.
(32) Sexton, L. T.; Horne, L. P.; Sherrill, S. A.; Bishop, G. W.; Baker, L. A.; Martin, C. R. Resistive-Pulse Studies of Proteins and Protein/Antibody Complexes Using a Conical Nanotube Sensor. *J. Am. Chem. Soc.* **2007**, *129*, 13144−13152.
(33) Han, A.; Creus, M.; Schurmann, G.; Linder, V.; Ward, T. R.; de Rooij, N. F.; Staufer, U. Label-Free Detection of Single Protein Molecules and Protein-Protein Interactions Using Synthetic Nanopores. *Anal. Chem.* **2008**, *80*, 4651−4658.
(34) Talaga, D. S.; Li, J. Single-Molecule Protein Unfolding in Solid State Nanopores. *J. Am. Chem. Soc.* **2009**, *131*, 9287−9297.
(35) Niedzwiecki, D. J.; Grazul, J.; Movileanu, L. Single-Molecule Observation of Protein Adsorption onto an Inorganic Surface. *J. Am. Chem. Soc.* **2010**, *132*, 10816−10822.
(36) Oukhaled, A.; Cressiot, B.; Bacri, L.; Pastoriza-Gallego, M.; Betton, J. M.; Bourhis, E.; Jede, R.; Gierak, J.; Auvray, L.; Pelta, J. Dynamics of Completely Unfolded and Native Proteins through Solid-State Nanopores as a Function of Electric Driving Force. *ACS Nano* **2011**, *5*, 3628−3638.
(37) Ledden, B.; Fologea, D.; Talaga, D. S.; Li, J. *Sensing Single Protein Molecules with Solid-State Nanopores*; Springer: New York, USA, 2011; pp 129−150.
(38) Yusko, E. C.; Johnson, J. M.; Majd, S.; Prangkio, P.; Rollings, R. C.; Li, J. L.; Yang, J.; Mayer, M. Controlling Protein Translocation through Nanopores with Bio-Inspired Fluid Walls. *Nat. Nanotechnol.* **2011**, *6*, 253−260.
(39) Cressiot, B.; Oukhaled, A.; Patriarche, G.; Pastoriza-Gallego, M.; Betton, J. M.; Auvray, L.; Muthukumar, M.; Bacri, L.; Pelta, J. Protein Transport through a Narrow Solid-State Nanopore at High Voltage: Experiments and Theory. *ACS Nano* **2012**, *6*, 6236−43.

DOI: 10.1021/acsnano.8b00734
ACS Nano 2018, 12, 4494−4502

(40) Wei, R.; Gatterdam, V.; Wieneke, R.; Tampe, R.; Rant, U. Stochastic Sensing of Proteins with Receptor-Modified Solid-State Nanopores. *Nat. Nanotechnol.* **2012**, *7*, 257−263.
(41) Yusko, E. C.; Prangkio, P.; Sept, D.; Rollings, R. C.; Li, J.; Mayer, M. Single-Particle Characterization of Aβ Oligomers in Solution. *ACS Nano* **2012**, *6*, 5909−5919.
(42) Freedman, K. J.; Haq, S. R.; Edel, J. B.; Jemth, P.; Kim, M. J. Single Molecule Unfolding and Stretching of Protein Domains inside a Solid-State Nanopore by Electric Field. *Sci. Rep.* **2013**, *3*, 1638.
(43) Plesa, C.; Kowalczyk, S. W.; Zinsmeester, R.; Grosberg, A. Y.; Rabin, Y.; Dekker, C. Fast Translocation of Proteins through Solid State Nanopores. *Nano Lett.* **2013**, *13*, 658−63.
(44) Larkin, J.; Henley, R. Y.; Muthukumar, M.; Rosenstein, J. K.; Wanunu, M. High-Bandwidth Protein Analysis Using Solid-State Nanopores. *Biophys. J.* **2014**, *106*, 696−704.
(45) Niedzwiecki, D. J.; Land, C. J.; Shemer, G.; Cheng, P. S.; Seven, J. G.; Drndic, M. Observing Changes in the Structure and Oligomerization State of a Helical Protein Dimer Using Solid-State Nanopores. *ACS Nano* **2015**, *9*, 8907−8915.
(46) Hu, R.; Diao, J.; Li, J.; Tang, Z.; Li, X.; Leitz, J.; Long, J.; Liu, J.; Yu, D.; Zhao, Q. Intrinsic and Membrane-Facilitated Alpha-Synuclein Oligomerization Revealed by Label-Free Detection through Solid-State Nanopores. *Sci. Rep.* **2016**, *6*, 20776.
(47) Yusko, E. C.; Bruhn, B. R.; Eggenberger, O. M.; Houghtaling, J.; Rollings, R. C.; Walsh, N. C.; Nandivada, S.; Pindrus, M.; Hall, A. R.; Sept, D.; Li, J.; Kalonia, D. S.; Mayer, M. Real-Time Shape Approximation and Fingerprinting of Single Proteins Using a Nanopore. *Nat. Nanotechnol.* **2017**, *12*, 360−367.
(48) Varongchayakul, N.; Huttner, D.; Grinstaff, M. W.; Meller, A. Sensing Native Protein Solution Structures Using a Solid-State Nanopore: Unraveling the States of Vegf. *Sci. Rep.* **2018**, *8*, 1017.
(49) Kowalczyk, S. W.; Hall, A. R.; Dekker, C. Detection of Local Protein Structures Along DNA Using Solid-State Nanopores. *Nano Lett.* **2010**, *10*, 324−8.
(50) Raillon, C.; Cousin, P.; Traversi, F.; Garcia-Cordero, E.; Hernandez, N.; Radenovic, A. Nanopore Detection of Single Molecule RNAP−DNA Transcription Complex. *Nano Lett.* **2012**, *12*, 1157−1164.
(51) Ivankin, A.; Carson, S.; Kinney, S. R.; Wanunu, M. Fast, Label-Free Force Spectroscopy of Histone-DNA Interactions in Individual Nucleosomes Using Nanopores. *J. Am. Chem. Soc.* **2013**, *135*, 15350−2.
(52) Bell, N. A. W.; Keyser, U. F. Specific Protein Detection Using Designed DNA Carriers and Nanopores. *J. Am. Chem. Soc.* **2015**, *137*, 2035−2041.
(53) Plesa, C.; Ruitenberg, J. W.; Witteveen, M. J.; Dekker, C. Detection of Individual Proteins Bound Along DNA Using Solid-State Nanopores. *Nano Lett.* **2015**, *15*, 3153−3158.
(54) Sze, J. Y. Y.; Ivanov, A. P.; Cass, A. E. G.; Edel, J. B. Single Molecule Multiplexed Nanopore Protein Screening in Human Serum Using Aptamer Modified DNA Carriers. *Nat. Commun.* **2017**, *8*, 1552.
(55) Waduge, P.; Hu, R.; Bandarkar, P.; Yamazaki, H.; Cressiot, B.; Zhao, Q.; Whitford, P. C.; Wanunu, M. Nanopore-Based Measurements of Protein Size, Fluctuations, and Conformational Changes. *ACS Nano* **2017**, *11*, 5706−5716.
(56) Goldberg, R. N.; Tewari, Y. B.; Bhat, T. N. Thermodynamics of Enzyme-Catalyzed Reactions - a Database for Quantitative Biochemistry. *Bioinformatics* **2004**, *20*, 2874−2877.
(57) Lienhard, G. E.; Secemski, I. I. P1,P5-Di(Adenosine-5′)-Pentaphosphate, a Potent Multisubstrate Inhibitor of Adenylate Kinase. *J. Biol. Chem.* **1973**, *248*, 1121−1123.
(58) Whitford, P. C.; Miyashita, O.; Levy, Y.; Onuchic, J. N. Conformational Transitions of Adenylate Kinase: Switching by Cracking. *J. Mol. Biol.* **2007**, *366*, 1661−71.
(59) Onuk, E.; Badger, J.; Wang, Y. J.; Bardhan, J.; Chishti, Y.; Akcakaya, M.; Brooks, D. H.; Erdogmus, D.; Minh, D. D. L.; Makowski, L. Effects of Catalytic Action and Ligand Binding on Conformational Ensembles of Adenylate Kinase. *Biochemistry* **2017**, *56*, 4559−4567.
(60) Lu, B.; Hoogerheide, D. P.; Zhao, Q.; Zhang, H.; Tang, Z.; Yu, D.; Golovchenko, J. A. Pressure-Controlled Motion of Single Polymers through Solid-State Nanopores. *Nano Lett.* **2013**, *13*, 3048−52.
(61) Li, J.; Hu, R.; Li, X.; Tong, X.; Yu, D.; Zhao, Q. Tiny Protein Detection Using Pressure through Solid-State Nanopores. *Electrophoresis* **2017**, *38*, 1130−1138.
(62) Schnell, J. R.; Dyson, H. J.; Wright, P. E. Structure, Dynamics, and Catalytic Function of Dihydrofolate Reductase. *Annu. Rev. Biophys. Biomol. Struct.* **2004**, *33*, 119−140.
(63) Schweitzer, B. I.; Dicker, A. P.; Bertino, J. R. Dihydrofolate-Reductase as a Therapeutic Target. *FASEB J.* **1990**, *4*, 2441−2452.
(64) Tabard-Cossa, V.; Trivedi, D.; Wiggin, M.; Jetha, N. N.; Marziali, A. Noise Analysis and Reduction in Solid-State Nanopores. *Nanotechnology* **2007**, *18*, 305505.
(65) Larkin, J.; Henley, R.; Bell, D. C.; Cohen-Karni, T.; Rosenstein, J. K.; Wanunu, M. Slow DNA Transport through Nanopores in Hafnium Oxide Membranes. *ACS Nano* **2013**, *7*, 10121−10128.
(66) Firnkes, M.; Pedone, D.; Knezevic, J.; Döblinger, M.; Rant, U. Electrically Facilitated Translocations of Proteins through Silicon Nitride Nanopores: Conjoint and Competitive Action of Diffusion, Electrophoresis, and Electroosmosis. *Nano Lett.* **2010**, *10*, 2162−2167.
(67) Cheneke, B. R.; Indic, M.; van den Berg, B.; Movileanu, L. An Outer Membrane Protein Undergoes Enthalpy- and Entropy-Driven Transitions. *Biochemistry* **2012**, *51*, 5348−5358.
(68) Kovermann, M.; Aden, J.; Grundstrom, C.; Sauer-Eriksson, A. E.; Sauer, U. H.; Wolf-Watz, M. Structural Basis for Catalytically Restrictive Dynamics of a High-Energy Enzyme State. *Nat. Commun.* **2015**, *6*, 7644.
(69) DeBlois, R. W.; Bean, C. P. Counting and Sizing of Submicron Particles by the Resistive Pulse Technique. *Rev. Sci. Instrum.* **1970**, *41*, 909−916.
(70) Frank-Kamenetskii, M. D.; Prakash, S. Fluctuations in the DNA Double Helix: A Critical Review. *Phys. Life Rev.* **2014**, *11*, 153−70.
(71) Teague, S. J. Implications of Protein Flexibility for Drug Discovery. *Nat. Rev. Drug Discovery* **2003**, *2*, 527−541.
(72) Benabbas, A.; Karunakaran, V.; Youn, H.; Poulos, T. L.; Champion, P. M. Effect of DNA Binding on Geminate CO Recombination Kinetics in CO-Sensing Transcription Factor COOA. *J. Biol. Chem.* **2012**, *287*, 21729−21740.

DOI: 10.1021/acsnano.8b00734
ACS Nano 2018, 12, 4494−4502